Acta Metallurgica, Vol. 28, pp. 757 to 770

0001-6160/80/0601-0757$02.00/0

ON THE GROWTH OF LENTICULAR MARTENSITE

MARC A. MEYERS

Department of Metallurgical Engineering, South Dakota School of Mines and Technology, Rapid City, South Dakota, U.S.A.

(*Received* 20 *April* 1979; *in revised form* 10 *October* 1979)

Abstract—It is proposed that the growth of lenticular martensite typically occurring in the Fe–Ni and Fe–C systems takes place by the propagation of waves throughout the material. Two different types of waves are postulated: longitudinal transformation waves and transverse transformation waves, propagating at velocities of the order of elastic waves. The longitudinal transformation wave initiates the transformation process, once an embryo has reached a critical size whereupon it becomes a nucleus; it propagates radially along directions contained in the habit plane, forming the mid-rib. The martensitic disc generated by the longitudinal transformation wave acts as a second-order nucleus for the transverse transformation. The term 'second-order nucleus' is used to distinguish it from the 'first-order nucleus' that gives rise to the start of the transformation. The transverse transformation waves propagate perpendicularly to the habit plane, starting at the mid-rib. Accordingly, different defect generation mechanisms operate along the longitudinal and transverse propagation directions, due to the differences in stress state and substructure at the fronts and propagation velocities. The model allows the determination of the shape of a growing martensite plate, which closely resembles lenticular martensite. If xz is the habit plane, the direction of transverse propagation is oy and the major shear direction is ox, the martensite lens can be described, at time t, by the equation

$$\frac{(x^2 + z^2)^{3/2}}{x^2 v_{ed} + z^2 v_{es}} - \frac{1}{k} \ln\left(1 - \frac{k|y|}{v_{es}}\right) = t$$

where v_{ed} and v_{es} are the velocities of longitudinal and shear elastic waves and k is a parameter. The arrest of growth takes place by uncoupling between the transformation front and the plastic waves that precede it. The implication of the pressure rise associated with the wave upon the nucleation is discussed.

Résumé—Nous pensons que la croissance de la martensite lenticulaire, dans les systèmes Fe–Ni et Fe–C par exemple, se produit par la propagation d'ondes dans le matériau. Nous proposons deux types d'ondes différents: des ondes de transformation longitudinale et transversale, qui se propagent à des vitesses proches de celles d'ondes élastiques. L'onde de transformation longitudinale provoque le début de la transformation, lorsqu'un germe a dépassé la taille critique; elle se propage radialement dans des directions du plan d'accolement, formant la côte médiane. Le disque de martensite produit par l'onde de transformation longitudinale joue à son tour le rôle d'un germe pour la transformation transversale. Nous parlons alors d'un 'germe du second ordre', afin de faire la différence avec le 'germe du premier ordre', qui a provoqué le début de la transformation. Les ondes de transformation transversales se propagent perpendiculairement au plan d'accolement, en partant de la côte médiane. En même temps, des défauts se forment selon divers mécanismes le long des directions de propagation longitudinale et transversale, du fait de différences dans les états de contrainte et de la sous-structure aux fronts et dans les vitesses de propagation. Ce modèle permet de déterminer la forme de la plaquette de martensite en cours de croissance: elle ressemble fortement à une martensite lenticulaire. Si xz est le plan d'accolement, la direction de propagation transversale est oy et la direction principale de cisaillement est ox; on peut alors décrire la martensite lenticulaire à l'instant t par l'équation:

$$\frac{(x^2 + z^2)^{3/2}}{x^2 v_{ed} + z^2 v_{es}} - \frac{1}{k} \ln\left(1 - \frac{k|y|}{v_{es}}\right) = t$$

où v_{ed} et v_{es} sont les vitesses des ondes élastiques longitudinale et de cisaillement, et où k est un paramètre. L'arrêt de la croissance se produit par découplage entre le front d'onde de transformation et les ondes de déformation plastique qui le précèdent. Nous discutons les conséquences sur la germination de l'augmentation de pression associée à l'onde.

Zusammenfassung—Es wird vorgeschlagen, daß das Wachstum der typischerweise in den Fe–Ni- und Fe–C-Legierungen vorkommenden linsenförmigen Martensiten über die Ausbreitung von Wellen im gesamten Material einsetzt. Zwei verschiedene Wellentypen werden postuliert: longitudinale und transversale Umwandlungswellen mit Ausbreitungsgeschwindigkeiten in der Größenordnung von elastischen Wellen. Die longitudinale Umwandlungswelle leitet den Umwandlungsprozess ein; wenn ein Embryo eine kritische Größe einmal erreicht hat, wird er ein Keim. Dieser vergrößert sich radial in Richtungen, die in der die Mittellinie bildenden Habitebene liegen. Der von der longitudinalen Welle gebildete Martensit wirkt als Keim zweiter Ordnung. Diese Bezeichnung wurde zur Unterscheidung vom Keim

Present address: Department of Metallurgical and Materials Engineering, New Mexico Institute of Mining and Technology, Socorro, New Mexico, U.S.A.

erster Ordnung, der die Umwandlung startet, gewählt. Die transversale Umwandlungswelle geht aus von der Mittellinie und breitet sich senkrecht zur Habitebene aus. Demzufolge laufen -hervorgerufen von den Unterschieden im Spannungszustand und in der Substruktur an den Fronten und den Unterschieden in den Ausbreitungsgeschwindigkeiten- verschiedene Mechanismen der Defekterzeugung entlang der longitudinalen und der transversalen Ausbreitungsrichtung ab. Das Modell erlaubt, die Form einer wachsenden Martensitplatte, die einem linsenförmigen Martensit weitgehend ähnelt, zu bestimmen. Mit xz die Habitebene, oy die Richtung der transversalen Ausbreitung und ox die Haupt-Scherrichtung kann die Martensitlinse zur Zeit t mit folgender Gleichung beschrieben werden:

$$\frac{(x^2 + z^2)^{3/2}}{x^2 v_{ed} + z^2 v_{es}} - \frac{1}{k} \ln\left(1 - \frac{k|y|}{v_{es}}\right) = t$$

v_{ed} und v_{es} sind die Geschwindigkeiten der elastischen longitudinalen und transversalen Wellen, k ist ein Parameter. Das Wachstum hört auf durch Entkoppeln von Umwandlungsfront und vorauslaufenden plastischen Wellen. Die Bedeutung des Druckanstieges durch die Welle auf die Keimbildung wird diskutiert.

1. INTRODUCTION

All other factors remaining constant, the velocity of a moving interface increases with increasing driving energy. The upper limit of this velocity is the velocity at which the atomic disturbances generated by the interface can be propagated throughout the material. The condensation shock [1, 2] is an example of a fast transformation (vapor–liquid) propagating in a wave-like fashion. In solid systems, martensitic transformations may propagate in a wave regime if sufficient driving energy is provided. Two types of elastic disturbances propagating at two characteristic velocities exist in solids: equivoluminal or shear waves (when the atomic displacements are perpendicular to the propagation direction) and dilatational or longitudinal waves (when the atomic displacements are parallel to the propagation direction). If the amplitudes of the waves exceed a certain critical value, one has, in general, plastic shear and shock waves. It is herein proposed that a moving interface in the martensitic transformation may propagate at velocities lower or equal to the above velocities. Accordingly, a transformation wave that establishes the upper limit for the propagation velocity is postulated. It is assumed that when the driving energy for the transformation is high enough, the velocity of transformation will reach this value; in this situation the transformation is said to propagate in a wave regime. A general mechanical disturbance propagates throughout a solid as two separate waves, traveling at well established velocities. A transformation produces atom displacements that are more complex than the ones generated by conventional waves, since all atoms cannot have identical displacement vectors. These atom displacements cannot be separated in displacements parallel and normal to the direction of propagation. Consequently, the velocity of the transformation wave will vary, depending on its propagation direction. It will be assumed that its initial value varies between the velocities of elastic dilatational and elastic shear waves:

$$v_{es} \leq v_t \leq v_{ed}.$$

If the direction of displacement of groups of atoms is close to the direction of propagation, $v_t = v_{ed}$. If the displacement of groups of atoms is approximately perpendicular to the propagation direction then $v_t = v_{es}$.

It should be emphasized that the concept of wave-like propagation of martensite is not new; in 1951 Machlin and Cohen [3] concluded that martensite growth in an Fe-30% Ni alloy took place by the propagation of a strain wave. The experiments conducted by Kulin and Cohen [4] corroborated this hypothesis. And, in 1955 Crussard [5] attempted to apply the shock-wave theory to the growth of martensite.

It is the objective of this paper to describe the growth of lenticular martensite in terms of the propagation of transformation waves. It is, of course, recognized that in only a fraction of the systems martensitic transformations take place under a wave regime. Thermoelastic martensite is known to grow slowly, and there is a dramatic decrease in the level of acoustic emission, as the carbon content of steel is decreased and the martensite morphology changes to lath [6]. Accordingly, the arguments developed in this paper apply to lenticular martensite characteristically occurring in Fe–Ni alloys (~30% Ni) and in steels with high carbon content. In particular, the calculations are conducted for a hypothetical Fe-30% Ni alloy with a {259} type habit plane. The velocities of dilatational and shear elastic waves for this alloy were computed by interpolating the elastic constants for iron and nickel and assuming isotropy; they were found to be 5780 and 3150 m/s, respectively. The strains introduced by the formation of a martensite lens and required to effect the transformation are complex and comprise the Bain strain, the rigid lattice rotation and the invariant strain. However, for the purpose of the arguments developed here, it will suffice to consider the macrostrains as composed of a shear of 0.20 along the habit plane and a dilatational strain of 0.05 normal to the habit plane. If the habit plane is taken as x–z, and the shear direction as ox, then one can express these strains, in the matrix form, as:

$$\begin{bmatrix} \epsilon_x & \frac{1}{2}\gamma_{xy} & \frac{1}{2}\gamma_{xz} \\ \frac{1}{2}\gamma_{xy} & \epsilon_y & \frac{1}{2}\gamma_{yz} \\ \frac{1}{2}\gamma_{xz} & \frac{1}{2}\gamma_{yz} & \epsilon_z \end{bmatrix} = \begin{bmatrix} 0 & 0.10 & 0 \\ 0.10 & 0.05 & 0 \\ 0 & 0 & 0 \end{bmatrix} \quad (1)$$

The above simplification allows one to consider two disturbances propagating ahead of a moving front: a uniaxial strain disturbance and a shear disturbance.

2. MODEL

Prior to the presentation of the model in terms of the combined propagation of waves in the longitudinal and transverse directions (Section 2.2) and of the mathematical description of the front profiles (Section 2.3), a few comments on nucleation are noteworthy.

2.1 *Nucleation*

At the outset, it is emphasized that no attempt is made here to correct or refute existing theories on martensitic nucleation. It is felt that the consideration of the dynamic nature of the phenomenon might help in the understanding of nucleation. If one views the embryos according to classical nucleation theory, then they are treated as transformation products already grown to a certain size [7]. An alternate approach is to consider the nucleus as forming instantaneously. If such is the case, then the lateral expansion ($\epsilon_y = 0.05$) is inhibited at time $t_0 = 0$. In other words, the nucleus is initially compressed until the expansion wave releases it. The extent of the stress generated by this initial compression is given by the Hugoniot curve for the alloy in question. This is actually a dynamic compressibility curve. One way of obtaining this curve is from the empirical linear relationship between particle and shock velocities U_p and U_s.

$$U_s = C + SU_p. \tag{2}$$

It is reasonable to obtain the coefficients C and S through an interpolation from the values for Fe and Ni [8]. One obtains:

$$C = 3.876 \times 10^5 \text{ cm/s}$$

$$S = 1.783$$

$$\rho_0 = 8.17 \text{ g/cm}^3 \text{ (initial density)}.$$

Applying equation 4.15 of Ref. [9], one obtains a relationship between the pressure and the ratio between the compressed volume V and initial volume V_0.

$$P = \frac{C\rho_0\left(1 - \frac{V}{V_0}\right)}{\left[1 - S\left(1 - \frac{V}{V_0}\right)\right]^2}. \tag{3}$$

In the state of uniaxial strain generated by ϵ_y, one has

$$\frac{V}{V_0} = (1 - \epsilon_x)(1 - \epsilon_y)(1 - \epsilon_z) \tag{4}$$

and

$$P = \frac{C\rho_0\epsilon_y}{(1 - S\epsilon_y)^2}. \tag{5}$$

Figure 1 shows the resulting dynamic compressibility

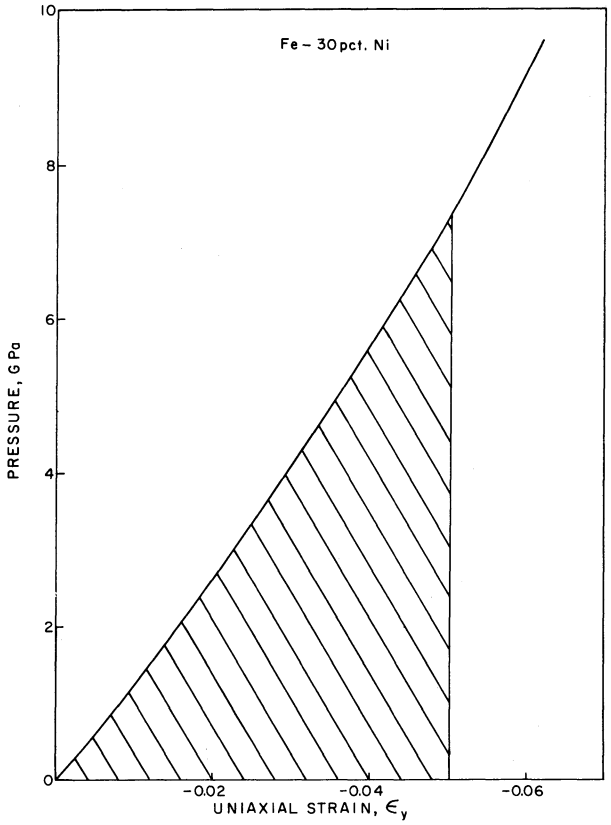

Fig. 1. Pressure vs uniaxial strain ϵ_y for an Fe-30% Ni alloy.

curve. The strains are indicated as negative in the abcissa because they are compressive. The uniaxial strain $\epsilon_y = 0.05$ will generate a pressure of 7.4 GPa; this pressure is well within the realm of shock waves. The cross-hatched area is equal to the energy released when the nucleus expands and the pressure is reduced (from 7.4 GPa) to zero. This energy is equal to 180 mJ/m^3. The shear component of the displacement and the interface will also contribute with an energy. Kaufman and Cohen [10] estimate these two terms to be equal to 38 mJ/m^3. Thus, the dilatational term cannot be neglected if one assumes that the nucleus forms instantaneously and the pressure builds up. Indeed, it could account for the large undercooling required ($T_0 - M_s \simeq 200$ K) in these alloys, while the undercooling required for thermoelastic martensites is of a few degrees. In effect, the change in free energy per K is of 0.72 mJ/m^3 − K in an Fe-30% Ni alloy and an undercooling of 250 K can be accounted by the pressure effect, assuming a 7.4 GPa maximum pressure. The dilatational strains in thermoelastic martensites are of the order of 0.005 (see Table 1 of Ref. [11]) and no significant pressures would be achieved. This might indeed be the critical difference between thermoelastic and 'irreversible' martensites.

Another point of concern is the thermodynamic criterion normally used in the classic developments; the use of the minimum Gibbs free energy as the equilibrium criterion only applies when the pressure is constant. The 'instantaneous' nucleation situation depicted above takes place under constant volume and temperature, and the Hemholtz free energy would be a more appropriate criterion, at time $t_0 = 0$. It is only when the expansion starts to occur, with an attendant decrease in P, that the temperature will change (actually, decrease). This expansion will be studied in greater detail in Section 2.2. The following expression is proposed for the net Hemholtz free energy difference between austenite and martensite per plate:

$$\Delta F = \Delta F_s + \Delta F_p + \Delta F_i + \Delta F_c. \qquad (6)$$

The subscripts s, p, i, and c refer to strain, pressure, interfacial energy, and chemical energy.

2.2 *Propagation*

The essential features of the proposed mechanism are presented in Fig. 2. The growth process is initiated when an embryo reaches a critical size. It proceeds by the coupled propagation of longitudinal and transverse transformation waves. The longitudinal transformation wave initiates the process. It radiates out of the nucleus along a specific crystallographic plane: the habit plane, Fig. 2(a). One could describe it as a second-order nucleus, as compared with the first-order nucleus required to activate the longitudinal transformation wave. The transverse transformation wave propagates perpendicularly to the habit plane; it initiates its course at the second-order nucleus and grows outwardly, on the two sides. Figure 2(b), in

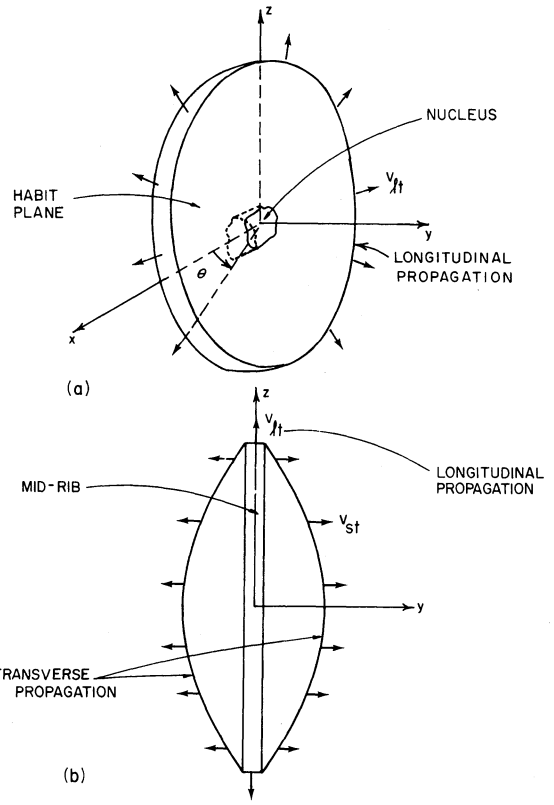

Fig. 2. Growth of martensite lens by wave propagation. (a) longitudinal propagation along plane xz at velocity v_{lt}, starting at nucleus; (b) transverse propagation with velocity v_{st}, perpendicular to habit plane (direction oy).

which a section was made perpendicular to the habit plane, shows both the longitudinal and transverse propagation. It is clear, in the present proposal, that the longitudinal wave produces the mid-rib and that the transverse wave produces the lateral sides of the martensite. Although the longitudinal and lateral growth take place concurrently, they will be described separately, in the next sub-sections.

2.2.1 *Longitudinal propagation.* Once the nucleus is formed, it will propagate along the undistorted and unrotated planes (habit planes) at a velocity v_{lt}. There are definite reasons why the propagation takes place along the habit plane. Reshuffling of the atoms is less severe along this plane and the energy required is less. Accordingly, the energy required for growth along another orientation would be larger. Referring to equation (1), one can see that the particle displacement can be expressed by γ_{xy}. So, in the ox direction the particle motion should be close to parallel to the propagation direction; in the oy direction, they should be perpendicular. One can therefore assume that:

$$(v_{lt})_{\theta=0} = v_{ed}$$
$$(v_{lt})_{\theta=\pi/2} = v_{es}. \qquad (7)$$

A continuous variation of velocities for intermediate orientations, between the above limits is given by a

cosine function.

$$(v_{lt})_\theta = \tfrac{1}{2}[(v_{ed} - v_{es})\cos 2\theta + v_{ed} + v_{es}]. \quad (8)$$

The configuration of the front after different propagation times is calculated in Section 2.3.

The atomic displacements at the longitudinal propagation front are, because of the inherent requirements of the transformation, more complex than in conventional elastic or plastic waves. They will not be analyzed in detail here, and a qualitative proposition will be made. The combined effect of the Bain strain, the invariant shear strain (equal to 0.25 according to Ref. [12]) and the lattice rotation would generate high shear stresses at the longitudinal front, if no relaxation mechanism were present. Multiplying the invariant shear strain by the shear modulus, one obtains a rough estimate of the stress level attained, if no accommodation took place. It would equal 15 GPa. However, these stresses can be accommodated by one or more of the following deformation modes.

(a) *Homogeneous dislocation nucleation.* The shear stress required for the homogeneous nucleation of a partial dislocation is roughly 5 GPa [13]. The shear stresses imposed at the longitudinal propagation front would be more than sufficient to nucleate them. In case dislocations are the carriers for the translation and rotation, a mechanism analogous to the one proposed by Meyers [14, 15] for shock waves is thought to be operative. Essentially, a shock front is a wave that transforms the virgin phase into a reduced lattice. Both phases have the same crystal structure, but different lattice parameters. The shear stresses that build up at the shock front are sufficient to homogeneously nucleate dislocations. Once generated, the dislocations do not advance with the front; these deviatoric stresses periodically build up again, giving rise to new dislocation interfaces.

Dislocation dynamical considerations do not have a bearing on the velocity of propagation of the longitudinal transformation wave because dislocations do not accompany the front. Dislocation *generation*, and not dislocation *motion* is responsible for the accommodation of the invariant lattice strains and rigid-body rotation. The dislocations are left behind the front and, therefore, have no bearing on its propagation. Meyers [15] discusses the effects of dislocation dynamics on the propagation of the shock front. The same arguments are valid for a transformation front.

(b) *Twinning.* Twin formation by homogeneous nucleation of the first loop of a partial dislocation is discussed by Hirth and Lothe [16]. The stress required for the first dislocation is the same as in item (a): around 5 GPa. However, the succeeding dislocations required for twinning have a much lower critical stress for nucleation: under 0.5 GPa.

(c) *Movement of existing dislocations.* If the longitudinal propagation front is moving into a lattice with a high dislocation density, movements of the existing dislocations can accommodate the high shear strains. Application of the Orowan equation shows the extent of motion. If the density of dislocations is of 10^{11} cm^{-2}, one has:

$$l = \frac{\gamma}{\rho b} = 0.83\,\mu m \quad (9)$$

where γ is the shear strain, ρ the dislocation density, b the Burgers vector and l the distance that each dislocation has to move. This distance is quite reasonable. The stress required to move existing dislocations is, of course, dependent on their velocity (e.g. Fig. 4 in Ref. [15]). Nevertheless, the dislocations can be displaced at sufficiently high velocities at stress levels substantially below the ones required for homogeneous dislocation or twin nucleation.

It should be noted that the conventional generation mechanisms, such as Frank-Read sources for dislocations and the pole mechanism for twinning were not considered. This is so because they would have to involve dislocation motion at velocities higher than the propagating longitudinal front. Consequently, the velocities of these dislocations would be necessarily in the supersonic range. Which one of the above three deformation modes would be preferred? In Fe–Ni alloys, the extent of twinning decreases with increasing amounts of deformation of the austenite [17, 18]. Although an explanation is provided by Johari and Thomas [17], an alternative explanation according to the deformation modes explained above, is that the movement of existing dislocations provided the means for the inhibition of the shear strains. And the experiments conducted by Rohde *et al.* [19] lend striking support to the proposed rationale. Upon shock-loading Ti-gettered iron, they found profuse twinning in the pre-annealed condition and total suppression of shock-induced twinning by prior cold work. Mahajan [20] obtained similar results upon shock-loading iron. So, the deviatoric stresses produced by a shock wave are accommodated by twinning when no dislocations are available and by motion of the already existing dislocations, if the iron is pre-deformed.

2.2.2 *Transverse propagation.* The martensitic region generated by the propagation of the longitudinal transformation wave acts as a second-order nucleus for the transverse growth of martensite. Equation 1 shows that once this nucleus forms, transverse propagation can take place, imposing the strains γ_{xy} and ϵ_y to the surrounding matrix. Since the phenomenon is dynamic, these plastic disturbances propagate in wave-like fashion. Thus, a plastic shear wave and a plastic shock wave are generated by the shear strain γ_{xy} and uniaxial strain ϵ_y, respectively. These two waves travel initially at velocities close to the velocities of elastic shear and dilatational waves, respectively; thus, the velocity of the shock wave is roughly twice that of the plastic shear wave that follows. If the nucleus would not induce transverse transformation, these waves would rapidly attenuate themselves after being emitted at time t_0. However, the passage of the shock and shear waves promotes the material transport required, as long as their amplitude is high

enough, so that a transverse transformation wave can closely follow them. This transverse transformation wave transforms—by means of organized atomic motions smaller than the interatomic spacing—the austenitic into the martensitic structure. The sequence of events as it is thought to occur is shown in Fig. 3(a–d). The transverse transformation wave moves perpendicularly to the habit plane; its course is initiated at the region transformed by the longitudinal wave. The two velocities v_{st} and v_{1t} are the transverse and longitudinal transformation wave velocities, respectively. It is seen in Fig. 3(a) how the plastic shear and shock waves precede the transformation wave. Figure 3(b) shows the instant at which the growth stops as the plastic shear and shock waves continue to advance [Fig. 3(c)]. However, because they are not energized by the transverse transformation wave any longer, they steadily attenuate themselves. This attenuation is of two sorts: (a) geometric attenuation, because the overall dimensions increase with roughly the square of the distance from the mid-rib plane (assuming a spherical wave front), and (b) dissipative attenuation, because of the energy required to create and move lattice defects along their path. After their amplitudes decrease below a critical value they become elastic waves. This is shown in Fig. 3(d). The dilatational wave has roughly twice the velocity of the shear wave; therefore, it precedes it. Another aspect of Fig. 3 that deserves attention is the process by which a hypothetical fiducial mark imbedded in the matrix is distorted. In Fig. 3(a) the plastic wave is shown to be responsible for the material transport that causes the distortion. The material transport becomes larger and larger, as the plastic waves advance [Fig. 3(b)]. But, once the transformation stops, the material transport steadily decreases, as the plastic waves attenuate themselves [Fig. 3(c)]. Figure 3(d) shows the final configuration of the fiducial mark. Regions very

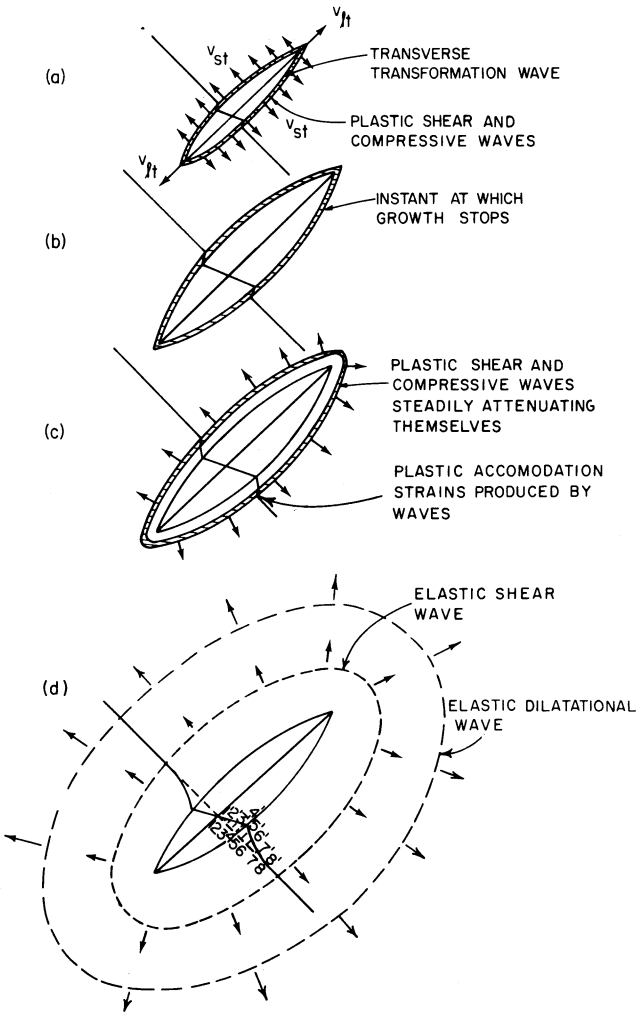

Fig. 3. Distortion of a hypothetical internal marker during propagation of martensite. (a) plastic shear and compression waves preceding transformation front; (b) and (c) after transverse propagation is arrested, plastic shear and compressive waves (shown coinciding) continue their course, steadily attenuating themselves; (d) after plastic waves underwent full attenuation to elastic shear and longitudinal waves, distortion of fiducial mark has the final shape. Observe plastic accommodation strains in front of final α–γ interface.

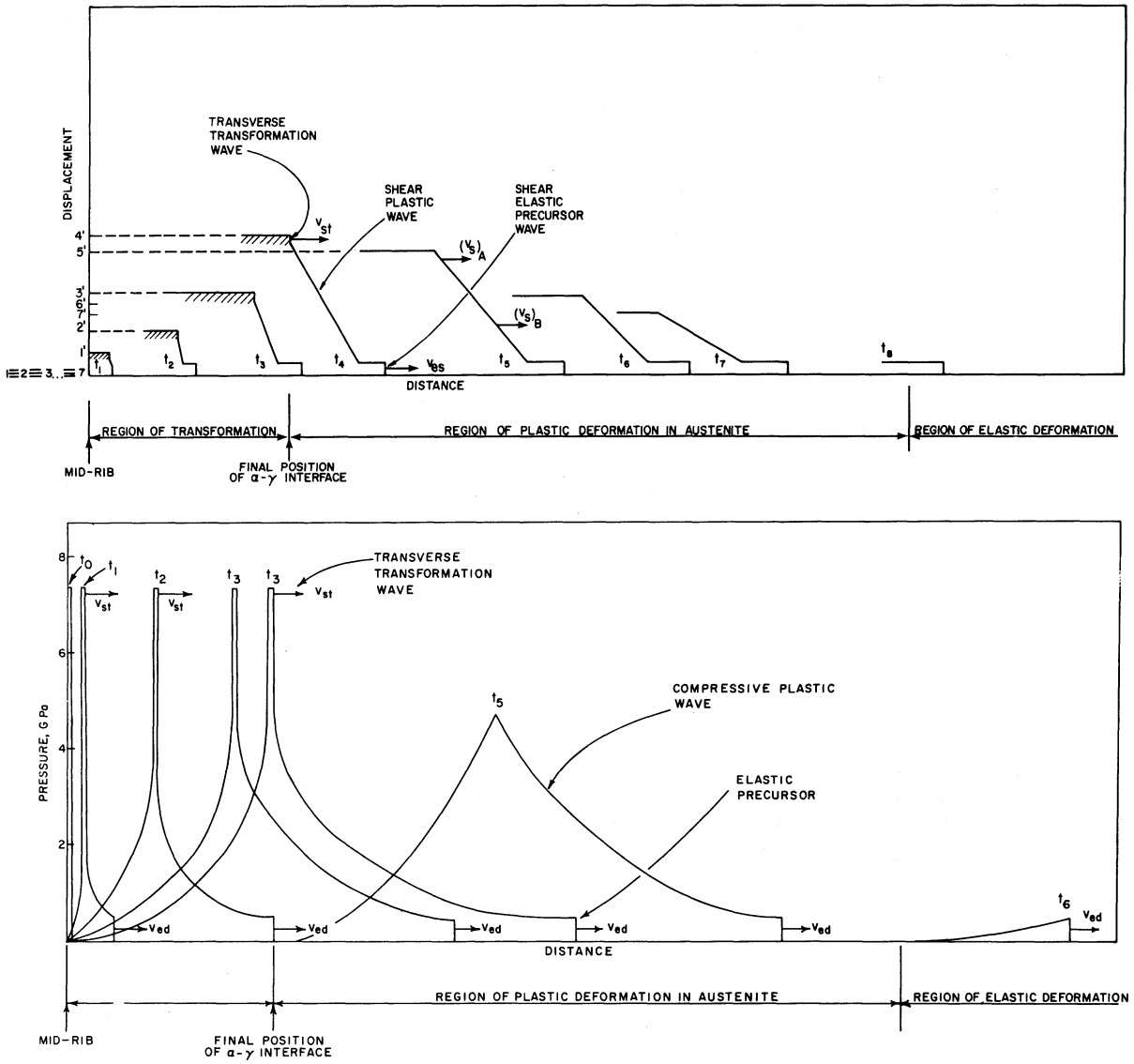

Fig. 4. (a) Lateral displacement vs distance (taken perpendicularly to habit plane) plot at various times t_1–t_8, corresponding to the displacements in Fig. 3(d); (b) pressure vs distance plot at various times t_1–t_8.

far away from the transformation are not affected, and therefore no distortion can be observed. However, as one approaches the austenite-martensite interface, the lines become increasingly distorted. Within the martensite plate, the line is rotated by ψ; due to the linearity of the transformation it remains straight. The point where the mid-rib intersects the line should be the center for the rotation of ψ. Points along the old trajectory (dashed line) are displaced to the new line. One has $1 \rightarrow 1'$, $2 \rightarrow 2'$, $3 \rightarrow 3'$, $4 \rightarrow 4'$, $5 \rightarrow 5'$, $6 \rightarrow 6'$, $7 \rightarrow 7'$. Actually, the lines $1 \rightarrow 1'$, $2 \rightarrow 2'$, $3 \rightarrow 3'$, $4 \rightarrow 4'$ are not parallel to the mid-rib; but one can assume them to be parallel, in the description that follows. So, macroscopic matter transfer has to take place. This transport is greater the farther the point is from the mid-rib. The submicroscopic atom shifts cannot perform this matter transference because atomic motions are less than an interatomic spacing. So, the plastic accommodation is produced on the larger scale by the plastic waves—mainly, the plastic shear wave—that precede the submicroscopic martensitic rearrangements.

Figure 4 shows the wave configurations at various times t_0–t_8 in greater detail. The times t_0–t_5 in Fig. 4 correspond to the instants at which the transformation front reaches points 0–5, in Fig. 3(d), while t_6, t_7, and t_8 correspond to the instants at which the top of the plastic shear front reaches points 6, 7, and 8, respectively. Both shear and compression plastic waves propagate ahead of the transformation. They are, however, presented separately in Fig. 4(a) and 4(b), respectively, for the sake of clarity. A qualitative description of their configuration and behavior is given in Fig. 4, as well as in the discussion below. The simultaneous generation of shock and shear waves has been theoretically treated by Bleich and Nelson [21]

and Ting and Nan [22] and was experimentally observed by Abou-Sayed *et al.* [23], but a rigorous analysis is not essential at the present level of understanding of the phenomenon. Figure 4(a) shows the progression of the leading plastic shear wave, while Fig. 4(b) shows the advance of the compressive wave due to the continuous emission of shock pulse from the transformation front. The displacements $1 \rightarrow 1'$, $2 \rightarrow 2'$, $3 \rightarrow 3'$, $4 \rightarrow 4'$, $5 \rightarrow 5'$, $6 \rightarrow 6'$, and $7 \rightarrow 7'$ correspond to the material transports shown in Fig. 3(d). Five types of waves are shown: in addition to the transverse transformation and plastic shear and compression waves, elastic shear and longitudinal waves (precursor waves) are shown; these waves do not have a substantial effect on the transformation. The displacements produced by them are much smaller than the ones produced by the plastic shear and compression waves and can probably be neglected. Along the distance axis, three regions can be discerned; a region of transformation (displacements 1–4), a region plastic deformation of the austenite (displacements 5–7) and a region of elastic deformation extending beyond displacement 8. From t_1–t_4, the displacement at the plastic shear wave increases linearly with distance (requirement for linear transformation). In this range, it carries the transformation wave [hatched region in Fig. 4(a)]. Beyond t_4 the shear wave does not trigger the transformation; the plastic wave no longer carries the transformation wave. Since it is no longer energized by the transformation wave, its amplitude decreases (t_5–t_7) until it becomes equal to the dynamic shear strength of the metal. Beyond that point it is merely an elastic shear wave. Figure 4(b) shows the compression vs distance plot; at time t_0 the nucleus is formed and (see section 2.1) the pressure suddenly rises to 7.4 GPa, because the strain $\epsilon_y = 0.05$ is inhibited. This produces a shock pulse with an extremely low duration (dictated by the thickness of the region). As the transformation wave advances, shock pulses of 7.4 GPa are continuously emitted and advance into the austenite, attenuating themselves and generating defects in the process. The situation is unique in that a moving shock-wave source travels through the matrix. The compressional wave front is therefore not steep but sloped, and it would be a misnomer to call this wave a 'shock' wave. A 'compression' wave is a better name.

An important feature of plastic shear waves is that they are not characterized by an abrupt front (see, for instance, Fig. 6 of Ref. [23]). This is due to the fact that larger shear displacements propagate at velocities lower than small ones (the inverse is true for shock waves). Thus, at time t_5 the velocity $(v_s)_A$ is lower than $(v_s)_B$, [Fig. 4(a)], because $(v_s)_A$ is at a higher displacement level. The slopes of the plastic shear front were assumed to be linear in Fig. 4(a), in accord with experimental measurements for 6061-T6 aluminum, reported by Abou-Sayed *et al.* [23, 24]. These slopes were assumed to decrease linearly, as the wave progresses through the material. This decrease in slope with time, due to a velocity dependence of displacement, has an important effect on the velocity of the transverse transformation wave. Since transformation can only occur at the top of the plastic shear wave, the velocity of the transverse transformation wave has to decrease with distance. Its initial value is the velocity of the elastic shear wave v_{es}. Assuming a linear decrease in slope of the plastic shear wave, then the velocity of the transverse transformation wave decreases linearly with distance. This is shown in Fig. 5, together with the distance dependence of the displacements labelled as they are in Fig. 3(d).

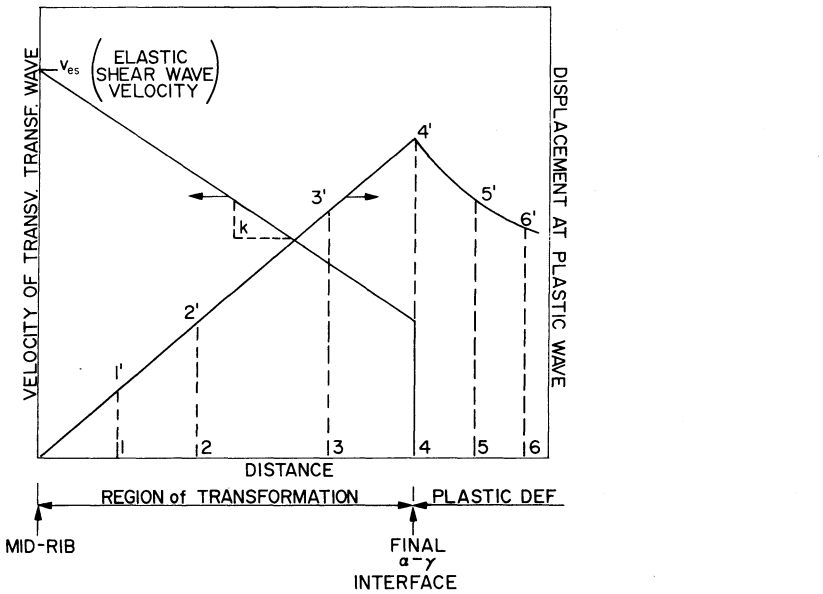

Fig. 5. Velocity of transverse transformation wave as a function of distance from plane of longitudinal propagation. Displacements of Fig. 3(d) shown on same plot.

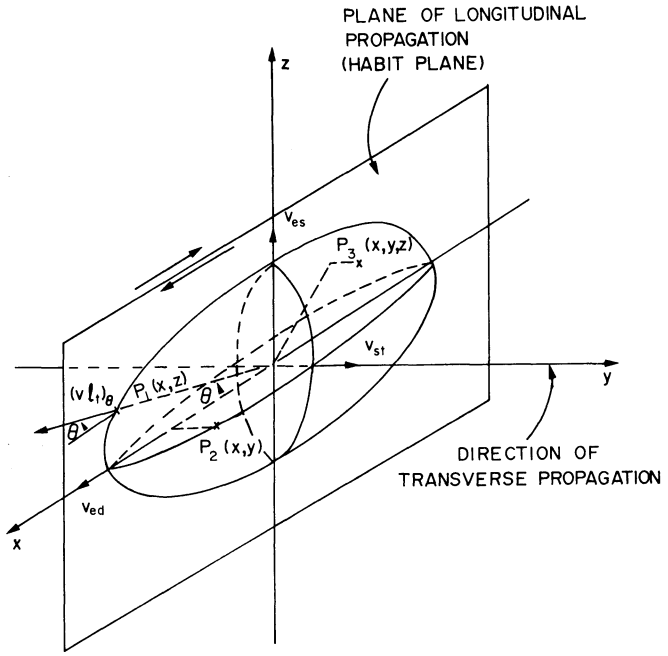

Fig. 6. Schematic representation of martensite lens during growth. Origin of axes coincides with position of embryo.

The displacements shown in Fig. 5 are accomplished by plastic deformation of the parent phase. It is interesting to observe that, since the shear wave precedes the transformation, the majority of the defects are generated in the parent phase and are then inherited by the martensitic structure. The transverse transformation front also might be responsible for the generation of a small fraction of these defects, because the austenite-martensite interface is not fully coherent; because it moves at high velocities, it is reasonable to think that these intrinsic interfacial dislocations are left behind and continually re-created as the front advances. Dislocation dynamical considerations (discussed in Ref. [15]) would point to this.

2.3 *Mathematical description*

It is relatively straightforward to describe the propagation of the front, once the velocities of the transformation wave along the various orientations are known. This will be done in this section. Figure 6 shows a martensite lens during propagation: the plane xy is the longitudinal propagation plane (shear direction ox) and oy is the direction of transverse propagation. The equation of the front profiles at the three planes xz (longitudinal propagation), yx, and yz (transverse propagation) will be calculated in the next three subsections. Then, the equation for the growing martensite lens will be derived.

2.3.1 *Plane of longitudinal propagation* (xz). At time t_i the longitudinal propagation front shown in Fig. 6 can be determined by substituting $(v_{lt})_\theta$ from equation (10)

$$x^2 + z^2 = (v_{lt})_\theta^2 t_i^2 \tag{10}$$

into equation (8):

$$x^2 + z^2 = t_i^2\left[\frac{(v_{ed} - v_{es})\cos 2\theta + v_{ed} + v_{es}}{2}\right]^2$$

But

$$\cos 2\theta = \cos^2\theta - \sin^2\theta$$

and

$$\cos\theta = \frac{x}{\sqrt{x^2 + z^2}}$$

$$\sin\theta = \frac{z}{\sqrt{x^2 + z^2}}$$

so:

$$(x^2 + z^2)^{3/2} - t_i(x^2 v_{ed} + z^2 v_{es}) = 0. \tag{12}$$

Equation (12) is plotted in Fig. 7(a) for four different times.

2.3.2 *Plane of transverse propagation* (xy). The plane xy is a diametral section with respect to the growth, started at instant t_0 when the embryo transformed into a nucleus. The shape shown in Fig. 6 is the shape at time t_i. The coordinates of point $P_2(x, y)$ at the instant t_i can be determined by the following calculations. The lateral growth at the ordinate (growth in the y direction) can only start once the longitudinal growth has extended to this region. Once the coordinates of (x, y) are known, the *locus* of the $P(x, y)$ points can be determined by making t vary from $t_0 = 0$ to t_i. The longitudinal displacement is given by:

$$|x| = v_{ed}t. \tag{13}$$

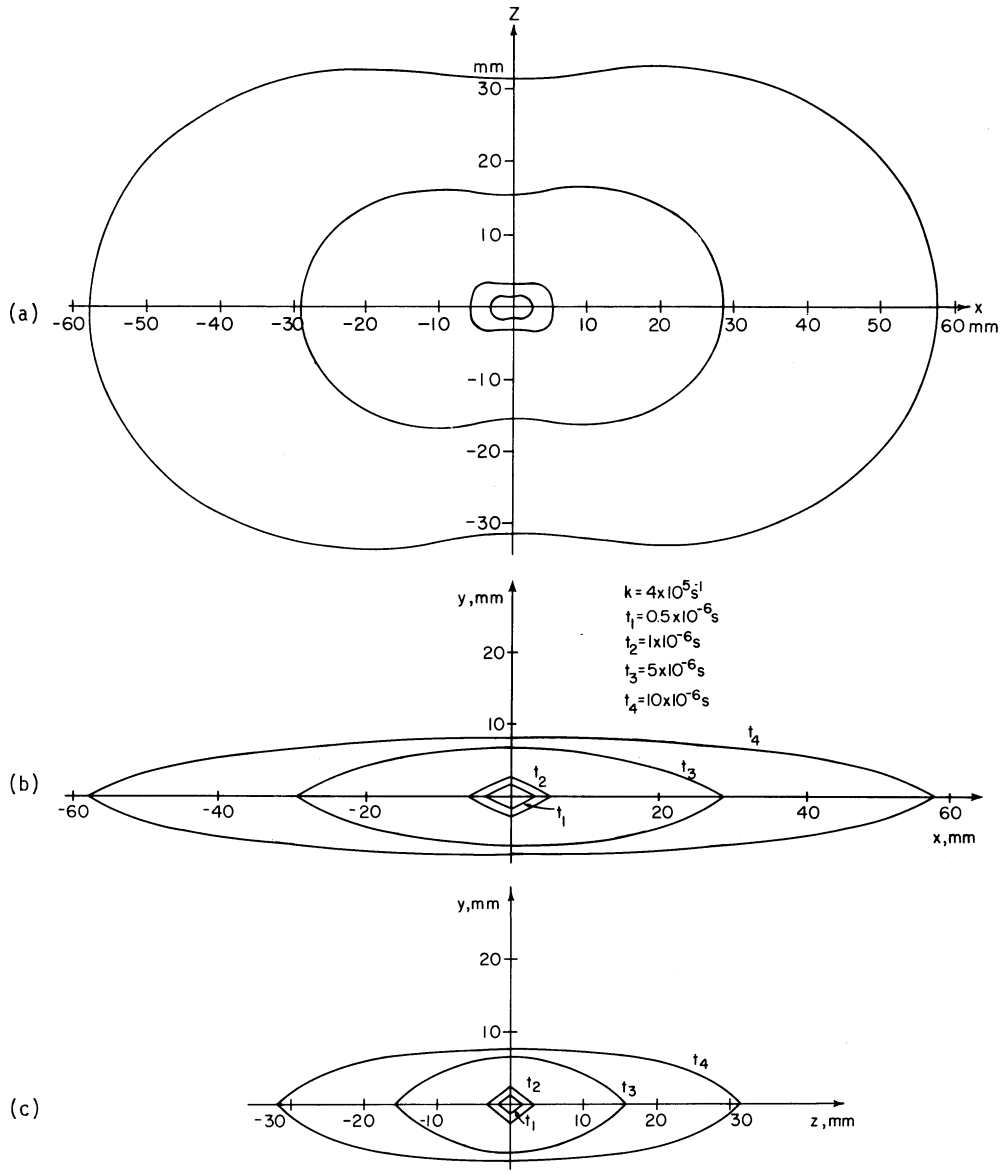

Fig. 7. Cross sections of martensite passing through origin at various times during growth ($k = 4 \times 10^5\ s^{-1}$); (a) longitudinal propagation (plane xz); (b) transverse propagation (plane xy); (c) transverse propagation (plane yz).

The transverse displacement is:

$$dy = v_{st}\, dt. \tag{14}$$

But the velocity of a transverse transformation wave decreases with the amount of shear required (see Fig. 5). It is assumed to decrease linearly with distance and the initial value is taken as the velocity of the elastic shear wave. Thus, it is expressed as:

$$v_{st} = v_{es} - k|y|. \tag{15}$$

Substituting equation (15) into equation (14):

$$dy = (v_{es} - k|y|)\, dt. \tag{16}$$

The differential equation is solvable by variable substitution. Making:

$$z = v_{es} - k|y| \tag{17}$$

$$dz = dv_{es} - k\, dy \tag{18}$$

or

$$dy = -dz/k. \tag{19}$$

Substituting equation (19) into equation (16), one obtains:

$$\ln z = -kt + c \tag{20}$$

or

$$\ln(v_{es} - k|y|) = -kt + c. \tag{21}$$

Applying the boundary condition: $t = t_i$ at $y = 0$

$$c = \ln v_{es} + kt_i. \tag{22}$$

Substituting equation (22) into equation (21):

$$\ln (v_{es} - k|y|) = -kt + \ln v_{es} + kt_i. \quad (23)$$

Substituting equation (13) into equation (23):

$$\ln\left(1 - \frac{k|y|}{v_{es}}\right) = k\left(\frac{|x|}{v_{ed}} - t_i\right). \quad (24)$$

2.3.3 *Plane of transverse propagation* (yz). Following the procedure delineated in Section 2.3.2, one obtains:

$$\ln\left(1 - \frac{k|y|}{v_{es}}\right) = k\left(\frac{|x|}{v_{es}} - t_i\right). \quad (25)$$

Equations (24) and (25) are plotted in Figs. 7(b) and 7(c), respectively, for four different values of time.

2.3.4 *Three-dimensional propagation.* Following the procedures delineated in Sections 2.3.1 through 2.3.3, it is possible to describe the growing martensite plate by means of a single equation. For this, it suffices to choose a general point P_3 (x, y, z) on the austenite-martensite interface (Fig. 6), and to consider the propagation as composed of a longitudinal term (from the origin to x, 0, z) and of a transverse term (from x, 0, z to x, y, z). The computation of the total time is made applying equations (12) and (16), by integrating the latter.

$$\frac{(x^2 + z^2)^{3/2}}{x^2 v_{ed} + z^2 v_{es}} - \frac{1}{k}\ln\left(1 - \frac{k|y|}{v_{es}}\right) = t_i. \quad (26)$$

Figure 8 shows a computer-generated perspective view of the martensite lens at time $t_i = 10^{-5}$ s.

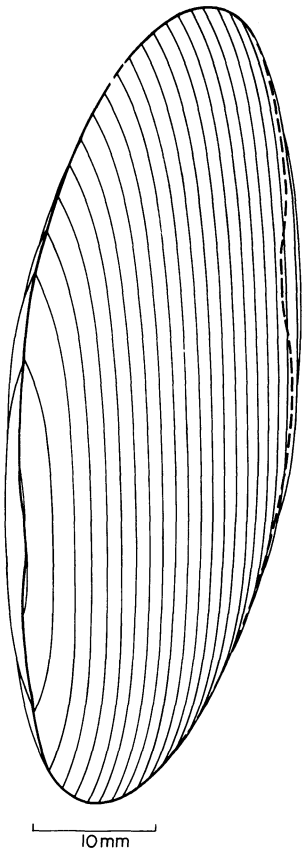

Fig. 8. Computer-generated perspective view of martensite lens at $t_i = 10^{-5}$ s.

2.4 *Final size and shape*

While the shape discussed in Section 2.3 (Figs 7 and 8) closely resembles lenticular martensite, it could very well not have any relationship with the final shape and size of the martensite, if the coupled growth ceases at a certain point, i.e. if the transformation front separates from the plastic waves that precede it, decelerating itself and advancing quasi-statically. Machlin and Cohen [3] showed that martensite plates did not thicken, once the temperature was decreased. This indicates that once plate growth is arrested it cannot restart, even if the chemical driving force is increased, and strongly suggests that dynamic factors are essential for growth.

Growth will be arrested if either the longitudinal or transverse propagation are inhibited. It will be assumed here that propagation stops immediately if the transformation front separates (the term 'uncouples' will be used) itself from the plastic waves that precede it. Once the uncoupling takes place in one region of the front, it has the ability to propagate itself along the front. Hence, if the growth of the plate is arrested at a point, this arrest propagates itself along the front.

Figure 9 shows a situation typical of a polycrystalline material: growth arrest is initiated when the longitudinal propagation is stopped by a grain boundary. The uncoupling front shown propagates along the transverse transformation front. This uncoupling front should have a velocity within the same range. The experimental observation that martensite plates with different sizes have fairly constant width/diameter ratios supports the contention that no portions of the front can freely propagate, once growth has stopped in an adjacent region. If such were the case, smaller (along the mid-rib) plates would have a proportionally greater thickness than large ones.

There are situations in which longitudinal propagation can proceed freely over relatively large distances (single crystals or specimens with large grain size). In this case, transverse propagation can be the size-determining factor. The transverse propagation situation is not a steady-state one, the velocity decreasing with propagation distance (Fig. 5). The amount of displacement preceding the front also increases with distance. Transverse propagation will stop when the work required to propagate the wave becomes greater than the free energy decrease due to the martensitic transformation. The free energy difference for a Fe-30% Ni alloy is approximately equal to $-120\,\mathrm{mJ/m^3}$ (-200 cal/mole [25]); hence the free energy per unit area of wave front gained by a front advance of dy is $(-120\,dy)\,\mathrm{mJ/m^2}$. On the other hand, the work required to advance the front by dy increases with the thickness y of the lens, because of

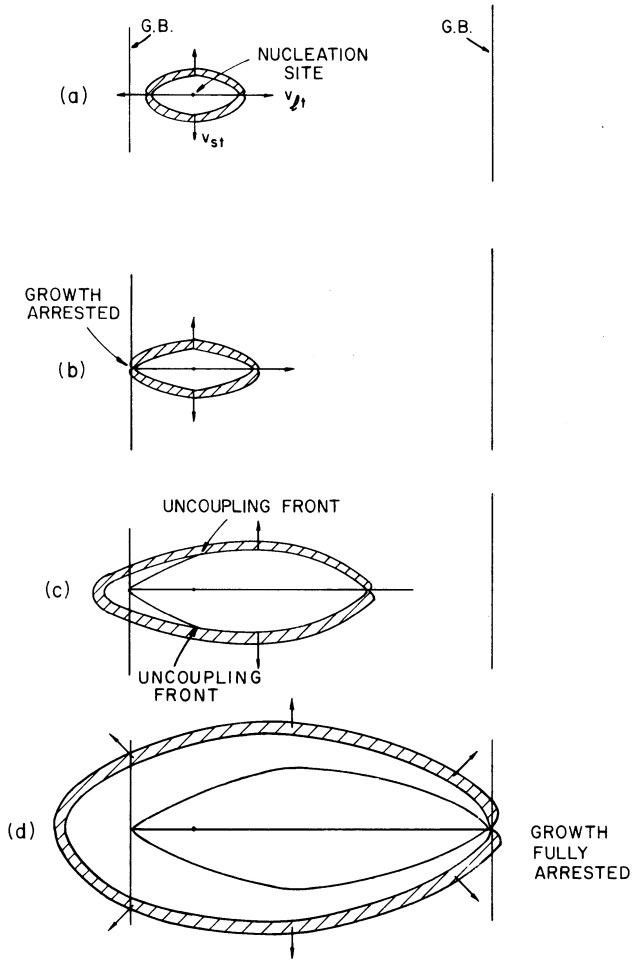

Fig. 9. Schematic representation of growth arrest in polycrystalline material.

the build-up of plastic waves that precede the transformation front. Once growth stops at a point—and, consequently, uncoupling takes place—this uncoupling will propagate along the front.

It should be noted that thermal effects were not considered in the above discussion. Thermal effects are very complex, because they involve temperature rise due to the release of chemical free energy and motion on dislocations as well as a temperature decrease due to the pressure decrease. They definitely have an effect on the mechanisms discussed above.

3. EXPERIMENTAL EVIDENCE

There is a considerable amount of information in the literature supporting the general features of the model proposed herein for the growth of martensite in terms of wave propagation. Some of this supportive evidence is briefly discussed below.

(a) The overall shape of lenticular martensite and the presence of a mid-rib are consistent with the proposed model.

(b) The proposition that the defects are generated in the austenite and then inherited by the martensite is supported by Crocker and Ross [26], and Krauss and Pitsch [27], who observed slip lines in the austenite surrounding a martensite plate. Additionally, McDougall and Bowles [28], and Jena and Wayman [29] observed striations in martensite inherited from the parent austenite.

(c) The low temperature dependence of growth velocity [4], as well as the fact that growth cannot be reinitiated once it is stopped [3] are consistent with a wave mechanism for propagation.

(d) The occurrence and inhibition of twinning can be explained by the strain rates, stress states and substructures encountered by the propagating transformation waves. The existence of a dislocation substructure seems to inhibit twinning. Consequently, predeformed materials tend to exhibit dislocations along the mid-rib. Even when twinning is prevalent at the mid-rib it often does not occur over the whole width of the lens. This is so because of two reasons: (a) the plastic waves that precede the transverse transformation wave generate more and more defects as they advance; (b) the transverse propagation velocity, and consequently strain rate decrease as the wave advances; twinning is known to be favored over dislo-

cation generation and motion at very high strain rates.

(e) The interactions observed between a propagating front and phosphide particles by Neuhauser and Pitsch [12] find a very clear explanation by the application of the concepts described herein; the 'shadows' of retained austenite are regions shielded from the plastic and transverse transformation waves by the particles. Similarly, jagged edges often encountered along the lateral interface of martensite can be very easily explained in terms of the ability of a plastic shear wave to propagate and to overcome obstacles.

(f) The burst phenomenon can be explained as the activation of embryos by the plastic waves (or the elastic precursor waves). These waves interact with existing boundaries, reinforcing themselves in certain regions [30].

(g) Bunshah and Mehl [31] observed an effect that they could not explain: in spite of the fact that the martensite has a lower electrical resistance than the austenite, the formation of the plate produced a high resistance spike, followed by the expected decrease in resistance. The adiabatic temperature rise alone ($\sim 110°C$) due to the energy released by the transformation could not account for the spike, which would correspond to a temperature increase of 1500°C, according to Bunshah and Mehl [31]. However, if one considers the effect of pressure on temperature and electrical resistance, one can explain the origin of the spike. During the propagation of the martensite plate, the pressure inside should be high, if shock waves are involved; this, in turn, produces a transient adiabatic temperature rise (just as in the compression of gases). A simple calculation will show the pressure required.

$$R_s = \left[R_{RT} + \left(\frac{\Delta R}{\Delta T}\right)\Delta T_T + \left(\frac{\Delta R}{\Delta T}\right)\Delta T_t \right]\frac{R_p}{R_0} \qquad (27)$$

where R_s is the resistance at the top of the spike; R_{RT}, the resistance at ambient temperature; ΔT_T, the temperature rise due to the transformation; ΔT_t, the transient temperature rise due to the pressure; R_p/R_0 is the ratio between the resistance at pressure P and the resistance at the pressure of one atmosphere. R_s, R_{RT}, and ΔT_T can be obtained from Bunshah and Mehl [31]; R_p/R_0 can be extrapolated from Lawson [32] (Table 12, column 5); ΔT_t is listed in Kinslow [33] for AISI 304 stainless steel. Inserting these values in equation (27), one has:

$$34.39 = [7.8 + 1.79 \times 10^{-2} \times 110 + 1.79 \times 10^{-2} \times \Delta T_t]\frac{R_p}{R_0}. \qquad (28)$$

By iteration for different values of the pressure one obtains the equality for a pressure of approximately 22 GPa. It is worth observing that R_p/R_0 is positive for an Fe-30% Ni alloy and is negative for Fe-20% Ni alloy. This reversal would lend itself very well to a critical experiment: the spike should be eliminated or sharply reduced for an Fe-20% Ni alloy.

7. CONCLUSIONS

In essence, the concepts described in the preceding sections allow the following conclusions to be drawn:

(a) A model for the growth of martensite by wave propagation is proposed. The model requires the postulation of longitudinal and transverse propagation waves.

(b) The longitudinal transformation wave initiates the growth process. It starts at the nucleus and propagates radially from it, in the habit plane. Its propagation velocity varies between the velocity of a dilatational elastic wave and that of an elastic shear wave in this medium.

(c) The transverse transformation wave propagates perpendicularly to the habit plane. The region transformed by the longitudinal transformation wave acts as a second-order nucleus for it. It grows initially with a velocity close to the velocity of elastic shear waves.

(d) The overall shape of the propagation front is calculated and is shown to strongly resemble lenticular martensite.

(e) Dislocation generation mechanisms at both the longitudinal and transverse propagation fronts are proposed.

(f) The interactions of transformation waves with plastic shear and shock waves and elastic dilatational and shear waves are discussed.

(g) The extent of plate growth is discussed in terms of energy expenditure and separation (uncoupling) of waves.

Acknowledgements—The author is indebted to a number of colleagues for helping him during the various stages of this investigation: G. A. Stone provided the idea from which these concepts germinated; stimulating discussions with C. Gruber, S. M. Howard, and G. B. Olson clarified many obscure points; C. Y. Hsu and K. C. Hsu developed the computer program used in the perspective view of the martensite lens; C. S. Barrett and J. R. C. Guimarães carefully read and thoughtfully annotated the manuscript. This work was supported by National Science Foundation Grant No. DMR77-28278.

REFERENCES

1. P. A. Thompson and D. A. Sullivan, *J. Fluid Mech.* **70,** 639 (1975).
2. P. A. Blythe and C. J. Shih, *J. Fluid Mech.* **76,** 593 (1976).
3. E. S. Machlin and M. Cohen, *Trans. AIME* **191,** 1019 (1951).
4. S. A. Kulin and M. Cohen, *Trans. AIME* **188,** 1139 (1950).
5. C. Crussard, *C.R., Acad. Sci. Paris* **240,** 2313 (1955).
6. G. R. Speich and A. J. Schwoeble, in *Monitoring Structural Integrity by Acoustic Emission*, p. 40 ASTM STP **571,** (1975).
7. Z. Nishiyama, *Martensitic Transformation.* p. 243, Academic Press, New York (1978).
8. R. G. McQueen, S. P. Marsh, J. W. Taylor, J. N. Fritz,

and W. J. Carter, in *High-Velocity Impact Phenomena* (edited by R. Kinslow), p. 293. Academic Press, New York (1970).
9. M. A. Meyers, Ph.D. Thesis, U. of Denver, Colorado, p. 62 (1974).
10. L. Kaufman and M. Cohen, in *Progress in Metal Physics* (edited by B. Chalmers and R. King), Vol. 7, p. 165. Pergamon Press, New York.
11. K. Shimizu and K. Otsuka, in *Shape Memory Effects* (edited by J. Perkins) p. 59. Plenum Press, (1975).
12. N. J. Neuhauser and W. Pitsch, *Acta Metall.* **19,** 337 (1971).
13. J. P. Hirth and J. Lothe, *Theory of Dislocations*, p. 689. McGraw-Hill, New York (1968).
14. M. A. Meyers, *Scripta Met.* **12,** 21 (1978).
15. M. A. Meyers, in *Strength of Metals and Alloys* (edited by P. Haasen, V. Gerold and G. Kostorz) p. 547. Pergamon Press, New York (1979).
16. Source cited in Ref. [13] p. 750.
17. O. Johari and G. Thomas, *Acta Metall.* **13,** 1211 (1965).
18. Source cited in Ref. [7] p. 37.
19. R. W. Rohde, W. C. Leslie and R. C. Glenn, *Metall. Trans.* **3A,** 323 (1972).
20. S. Mahajan, *Phys. stat. sol.* **33,** 291 (1969).
21. H. H. Bleich and I. Nelson, *J. appl. Mech.* **33,** 149 (1966).
22. T. C. T. Ting and N. Nan, *J. appl. Mech.* **36,** 189 (1969).
23. A. S. Abou-Sayed, R. J. Clifton and L. Hermann, *Expl. Mech.* **16,** 127 (1976).
24. A. S. Abou-Sayed and R. J. Clifton, *J. appl. Mech.* **44,** 79, 85 (1977).
25. J. R. Patel and M. Cohen, *Acta Metall.* **1,** 531 (1953).
26. A. G. Crocker and N. D. H. Ross, *Inst. Metals Monogr.* No. **33,** p. 176 (1969).
27. G. Krauss and W. Pitsch, *Arch. Eisenhüttenwes.* **35,** 667 (1964).
28. P. G. McDougall and J. S. Bowles, *Acta metall.* **12,** 779 (1964).
29. S. Jena and C. M. Wayman, *Metall. Trans.* **1,** 2815, 2825 (1970).
30. M. A. Meyers, *Mater. Sci. Engng.* **30,** 99 (1977).
31. R. F. Bunshah and R. F. Mehl, *J. Metals* **5,** 1251 (1953).
32. A. W. Lawson, in *Progress in Metal Physics* (edited by B. Chalmers and R. King), Vol. 6, p. 1. Pergamon Press, London (1956).
33. R. Kinslow (editor), *High-Velocity Impact Phemonena*, p. 551. Academic Press, New York (1970).